

Water assisted gate induced temporal surface charge distribution probed by electrostatic force microscopy

Y. Pascal-Levy, E. Shifman, I. Sivan, I. Kalifa, M. Pal-Chowdhury et al.

Citation: *J. Appl. Phys.* **112**, 084329 (2012); doi: 10.1063/1.4761981

View online: <http://dx.doi.org/10.1063/1.4761981>

View Table of Contents: <http://jap.aip.org/resource/1/JAPIAU/v112/i8>

Published by the [American Institute of Physics](#).

Related Articles

Influence of target composition and deposition temperature on the domain structure of BiFeO₃ thin films
[AIP Advances 2, 042104 \(2012\)](#)

Nanodomain structures formation during polarization reversal in uniform electric field in strontium barium niobate single crystals

[J. Appl. Phys. 112, 064117 \(2012\)](#)

The effect of the top electrode interface on the hysteretic behavior of epitaxial ferroelectric Pb(Zr,Ti)O₃ thin films with bottom SrRuO₃ electrode

[J. Appl. Phys. 112, 064116 \(2012\)](#)

Ferroelectric vs. structural properties of large-distance sputtered epitaxial LSMO/PZT heterostructures
[AIP Advances 2, 032184 \(2012\)](#)

Piezoelectric nonlinearity and frequency dispersion of the direct piezoelectric response of BiFeO₃ ceramics
[J. Appl. Phys. 112, 064114 \(2012\)](#)

Additional information on J. Appl. Phys.

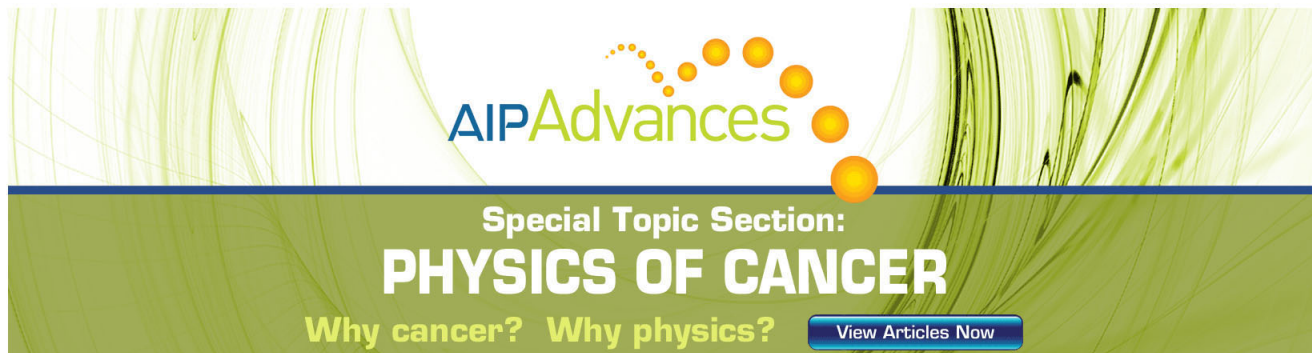
Journal Homepage: <http://jap.aip.org/>

Journal Information: http://jap.aip.org/about/about_the_journal

Top downloads: http://jap.aip.org/features/most_downloaded

Information for Authors: <http://jap.aip.org/authors>

ADVERTISEMENT



AIP Advances

Special Topic Section:
PHYSICS OF CANCER

Why cancer? Why physics? [View Articles Now](#)

Water assisted gate induced temporal surface charge distribution probed by electrostatic force microscopy

Y. Pascal-Levy,^{1,2} E. Shifman,² I. Sivan,³ I. Kalifa,² M. Pal-Chowdhury,² O. Shtempluck,² A. Razin,² V. Kochetkov,² and Y. E. Yaish^{2,a)}

¹Russell Berrie Nanotechnology Institute, Technion, Haifa 32000, Israel

²Department of Electrical Engineering, Technion, Haifa 32000, Israel

³Department of Physics, Technion, Haifa 32000, Israel

(Received 30 May 2012; accepted 3 October 2012; published online 25 October 2012)

In this paper, we present a quantitative method to measure charge density on dielectric layers using electrostatic force microscopy. As opposed to previous reports, our method, which is based on force curve measurements, does not require preliminary knowledge of the tip-sample capacitance and its derivatives. Using this approach, we have been able to quantify lateral and temporal SiO₂ surface charge distribution and have unveiled a gate-induced charge redistribution mechanism which takes place in the vicinity of grounded electrodes. We argue that this mechanism constitutes a dominant factor in the hysteresis phenomenon, which is frequently observed in the transfer characteristics of nano-scale devices. © 2012 American Institute of Physics. [<http://dx.doi.org/10.1063/1.4761981>]

I. INTRODUCTION

One promising direction for the transistors of the future involves nano-scale electronics, in which the active part of the device is of nano-scale dimensions. One example of such devices is carbon nanotube field effect transistors (CNTFETs), which have been the subject of many studies due to their excellent performance and high sensitivity to various analytes. Still, there are some unresolved issues related to their gate-modulated conductance, commonly measured through their transfer characteristics. During these measurements, appreciable hysteresis has often been observed between the forward and the reverse sweeping directions of the gate voltage, resulting in erroneous estimation of the device properties. Since hysteresis involves the movement of charges, it is appealing to use electrostatic force microscopy (EFM) in order to gain additional information regarding this phenomenon.

EFM is a powerful scanning probe technique that can be used to perform non-destructive, local electrostatic force measurements on a submicrometric scale. In the last decade, EFM has been used to explore a wide range of electrical properties, among which surface potential, contact potential,¹ charge distribution,²⁻⁴ dielectric constant,⁵ and conducting properties.⁶⁻⁸ EFM has also been used to inject charge and study its distribution in various types of samples, such as Co and Si nanoclusters embedded in conductive⁹ and non-conductive substrates,^{10,11} semiconductor nanoparticles,¹² oxide^{13,14} and alumina films,¹⁵ quantum dots,^{16,17} and carbon nanotubes.^{18,19}

Briefly, EFM is a dual pass technique: in the first line scan the tip operates in tapping mode, acquiring a topography profile of the sample surface. In the second line scan (interleave), the topographic data are used to retrace the first scan while the tip travels at a defined height above the surface. During the second scan the cantilever oscillates at its

resonant frequency, and a DC voltage is applied to the tip with respect to the substrate. The phase difference between the driving force and the observed oscillation of the tip is measured as a function of the tip position. This phase, ϕ , is proportional to the gradient of the force F between the tip and the sample in the vertical direction z

$$\phi = -\frac{Q}{k} \frac{\partial F}{\partial z}, \quad (1)$$

where Q is the quality factor and k is the spring constant of the tip.

Possible system configuration which we have adopted in this study and is relevant for understanding the hysteresis phenomenon and temporal charge distributions consists of surface charge which is deposited on an insulating layer (for example, SiO₂) lying on top of highly doped silicon back gate. Previous studies have shown that the total electrostatic forces acting between an EFM tip and a substrate are composed of capacitive forces associated with the tip-sample potential difference and Coulombic forces induced by the static charges on the surface. A generalized expression is given by

$$\frac{\partial F}{\partial z} = \frac{1}{2} \frac{d^2 C}{dz^2} (\Delta V)^2 + \alpha (\Delta V) Q_s + \beta Q_s^2, \quad (2)$$

where C is the capacitance between the tip and the sample, ΔV is the tip-sample potential difference, Q_s is surface charge, and α and β are coefficients which depend on z and on C and its derivatives. A wide variety of versions for this generalized equation exists in the literature, differing in α and β definitions. For example, in paper by Jespersen and Nygard²⁰

$$\alpha = \frac{1}{2\pi\epsilon_0 z^2} \left[\frac{C}{z} - \frac{1}{2} \frac{\partial C}{\partial z} \right],$$

$$\beta = \frac{A}{2\pi\epsilon_0 z^3},$$

^{a)}Electronic mail: yuvaly@ee.technion.ac.il.

where ϵ_0 is the vacuum permittivity and $A \in (0, 1)$ describes the relative distribution of the image charges between the tip and the substrate.

One problematic point in Eq. (2) lies on how one determines C and its derivatives, as the tip-surface configuration is geometrically complex. Many authors have tried to overcome this obstacle by using the plane-plane capacitor model, in which

$$C = \frac{S\epsilon_0}{z + \frac{t}{\epsilon_s}}, \quad (3)$$

where S is the effective plate area, ϵ_0 is the vacuum permittivity, and t and ϵ_s are, respectively, the thickness and the dielectric constant of the insulating layer. However, this simplification is of course far from being accurate and raises yet another difficulty: the determination of an equivalent plate area S . A different approach was adopted by Hudlet *et al.*,²¹ who proposed an analytical model to determine the tip-surface force. However, the obtained expression applies only for metallic surfaces and is approximated as well. When we tried to use it to determine the capacitance between the tip and a gold surface, we found it to be only partially compatible with our data.

A second obstacle arising from Eq. (2) is the determination of the effective tip-sample separation distance z . In the literature, z is often set as the apparent lift height (z_0) in which the second EFM scan is conducted. However, the apparent height changes while the tip-sample voltage is being modified. Therefore, if the surface is charged, the topographic data of the first scan might be erroneous, resulting in z_0 which is considerably different than the real separation distance z .

Below we present an alternative method to gain quantitative information on surface charge without the need to use the tip-surface capacitance and its derivatives. Furthermore, since our method involves performance of dynamic force curves measurements over the charged substrate, we are able to extract the accurate vertical distance z from the piezo displacement and the tip deflection. Having developed this method, we use the capabilities of the EFM to image migrating surface charge on SiO_2 . We have found that redistribution of the charge is a direct result of the gate bias, it takes place in the vicinity of electrodes due to the formation of lateral electric fields, and it is strongly influenced by humidity. Since the accumulating charge can gradually screen the gate, we argue that non-passivated nano-devices, which are frequently used for sensing applications, such as CNTFETs, can be influenced by this phenomenon and suggest that gate-induced surface charge redistribution is partially responsible for the hysteresis in such devices. Our model is confirmed by simulations performed with a finite element analysis software (COMSOL Multiphysics 4.2a), and its implications are discussed.

II. EXPERIMENTAL

Force curves measurement technique consists in recording the cantilever deflection when the tip approaches at

constant speed towards the surface, above a fixed point of the sample, and then retracts. During this measurement the feedback loop is turned off. Combining the piezo movement and the tip deflection enable us to determine the exact location of the tip above the surface. Other tip parameters, such as amplitude and phase, are also recorded as a function of z during the force curve measurement. Standard EFM phase measurements (lateral scans at a fixed z) were performed as described in the main text.

The samples we used had 500 nm of thermally grown SiO_2 layer on top of highly p-doped Si substrates. Pairs of electrodes (540 nm Cr\textit{p}t) with 10 μm gaps were patterned using photolithography techniques. All experiments were performed in ambient conditions; ambient humidity was monitored using a conventional humidity sensor. Ozone treatment was performed in 120 $^\circ\text{C}$ for 10 min.

Experiments were performed on a commercial AFM Nanoscope V Dimension 3100 from Veeco Instruments. The cantilevers we have used were manufactured by Mikro-Masch, with triangular shape, 200 μm in length and 40 μm in width, nominal spring constant of 3 N/m, and resonant frequencies in the range of 45-75 kHz. The quality factor Q is approximately 250. The tips were made of Si coated with Cr-Au to ensure a metallic behavior, and their nominal radius of curvature is less than 50 nm. A schematic representation of the experimental setup is depicted in Fig. 1.

III. RESULTS AND DISCUSSION

Fig. 2 shows a schematic of the tip-charged sample configuration. The static surface charge density Q_s on the surface of the SiO_2 induces image surface charge densities Q_{tip} and Q_g on the tip and the gate, respectively. Taking the two series capacitors (where C_0 and C_{ox} are the tip-surface and surface-gate capacitors, respectively) as well as the energy associated with the power sources into consideration, the total energy of the system per unit area can be expressed as follows:

$$\epsilon = \frac{1}{2} \frac{Q_g^2}{C_{ox}} - V_g Q_g + \frac{1}{2} \frac{Q_{tip}^2}{C_0} - V_{tip} Q_{tip}. \quad (4)$$

Imposing charge conservation and Kirchoff's law, one can express Q_{tip} and Q_g as a function of Q_s and the external biases

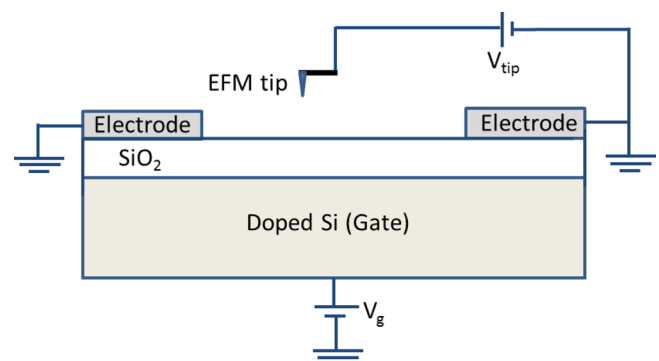


FIG. 1. A schematic of the experimental setup.

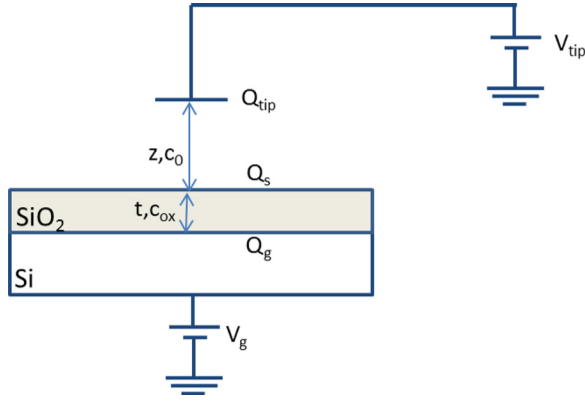


FIG. 2. Schematic representation of the tip-charged sample system configuration.

$$Q_{tip} = \frac{-C_0 Q_s + C_0 C_{ox} (V_g - V_{tip})}{C_0 + C_{ox}}, \quad (5)$$

$$Q_g = \frac{C_0}{C_0 + C_{ox}} (-Q_s + C_0 (V_g - V_{tip})).$$

Inserting these expressions of Q_{tip} and Q_g back into the energy expression (Eq. (4)) and taking the second derivative with respect to z , yield the final result

$$\frac{\partial F}{\partial z} = -\frac{1}{2(C_{ox} + C_0)^3} (Q_s + C_{ox} (V_g - V_{tip}))^2 \times \left[-2 \left(\frac{\partial C_{ox}}{\partial z} \right)^2 + \frac{\partial^2 C_0}{\partial z^2} (C_{ox} + C_0) \right]. \quad (6)$$

For a given distance, z , C_0 is constant, and the obtained expression depends quadratically on $(V_g - V_{tip})$. Once the minimum of the parabola is found, the calculation of the surface charge per unit area, Q_s , is straightforward

$$Q_s = -C_{ox} (V_g - V_{tip})_{min} = -\frac{\epsilon_0 \epsilon_{ox}}{t} (V_g - V_{tip})_{min}. \quad (7)$$

The same expression for Q_s (but with a different derivation) can be found in Marchi *et al.*²² It should be mentioned that the same derivation and final expression apply for charge which is uniformly spread in the bulk of the SiO_2 as well ($Q = \rho t$).

In order to confirm the validity of Eq. (6), force curve measurements using different tip voltages were performed on a pristine, highly doped silicon wafer with 500 nm thermally grown SiO_2 . Since this wafer did not pass any process at all, we expected to have no surface charge distribution, whatever. First, the measurements were performed while applying zero voltage to the gate, V_g (Fig. 3(a)). Next, a voltage of +2 V was applied to the gate, and the measurements were conducted again (Fig. 3(b)). One can observe that for zero gate voltage, the curves for $V_{tip} = +2, -2$ V are nearly identical, and likewise the curves for $V_{tip} = +3, -3$ V. When applying a voltage of $V_g = +2$ V, on the other hand, the $V_{tip} = -1, +5$ V curves become identical, same as the $V_{tip} = +4, 0$ V curves. To clarify these results further we depict $\partial F/\partial z$ as a function of $V_g - V_{tip}$ for $z = 100$ nm, and

for $V_g = 0$ V and $V_g = 2$ V, in Figs. 3(c) and 3(d), respectively. The dependence is indeed parabolic, and one can observe that the minima of the parabolas are very close to 0 V (0.055 ± 0.014 V and 0.041 ± 0.012 V for $V_g = 0$ V and $V_g = 2$ V, respectively), i.e., $V_g \simeq V_{tip}$, as expected according to Eq. (6) in the absence of surface charge (we ignore small work function difference between the tip and the silicon substrate).

However, on the same wafer that undergoes 10 min of ozone treatment the results were different. Fig. 4 depicts $\partial F/\partial z$ vs the potential difference, $V_g - V_{tip}$, for zero gate bias. It is evident from the data that the parabola minimum is located at $V_{tip} = -0.46 \pm 0.078$ V, which implies surface charge density of $Q_s = -3.22 \times 10^{-9} \pm 5.38 \times 10^{-10}$ C/cm², which is a typical value for ozone cleaner. For more aggressive treatment in oxygen plasma the shift in the parabola minimum was much bigger, indicating larger surface charge which accumulates on the substrate.

Having confidence with the discussed method, we can address the question regarding the influence of the gate on nano-scale transistors. For that purpose, we performed force curve measurements on a sample on which a pair of electrodes was lithography patterned. These two electrodes were grounded, and the measurements were performed for three different V_g : 0V, +2V, -2V and were taken approximately in the center of the gap between the electrodes. Data of $\partial F/\partial z$ at $z = 100$ nm are shown in Fig. 5 as a function of $V_g - V_{tip}$. One can observe that when $V_g = 0$ V, the parabola is nearly symmetrical around the $V_g - V_{tip}$ axis, indicating a minute amount of local charge on the surface, as in the case of uncharged samples ($Q_s = -2.89 \times 10^{-10} \pm 9.24 \times 10^{-11}$ C/cm²). However, when a voltage is applied to the gate, clear shifts are visible in the minima of the parabolas, indicating that charge has been redistributed on the surface of the sample at the examined point ($Q_s = -1.12 \times 10^{-8} \pm 1.75 \times 10^{-9}$ C/cm² and $Q_s = 9.59 \times 10^{-9} \pm 1.42 \times 10^{-9}$ C/cm² for $V_g = +2$ V and -2 V, respectively).

Interestingly, for low gate voltages, this induced surface charge depends linearly on V_g . Fig. 6 depicts the resulted Q_s for different V_g measured between two grounded electrodes. The red triangles were extracted from the force curve-based method we have introduced before. The green squares were found using conventional EFM phase imaging at $z = 100$ nm above the surface and extracting Q_s from Eq. (6) using the plane-plane capacitor approximation. The black circles were measured in the same method as for the green squares, but omitting the Q_s^2 term from Eq. (6) when calculating Q_s as has been done in a number of previous studies.^{23–25} It can be seen that the results which are derived from the force curve-based method are in reasonable agreement with the results obtained from the standard EFM measurements as long as Q_s is calculated using Eq. (6) as a whole. The slight dissimilarity observed between the two sets of results probably arises from the tip-plane capacitor approximation, as well as from inaccurate value of the height, z , above the sample where the standard EFM phase measurements have been performed. When the Q_s^2 term is omitted, however, results are erroneous, as expected, with an increasing error as V_g increases.

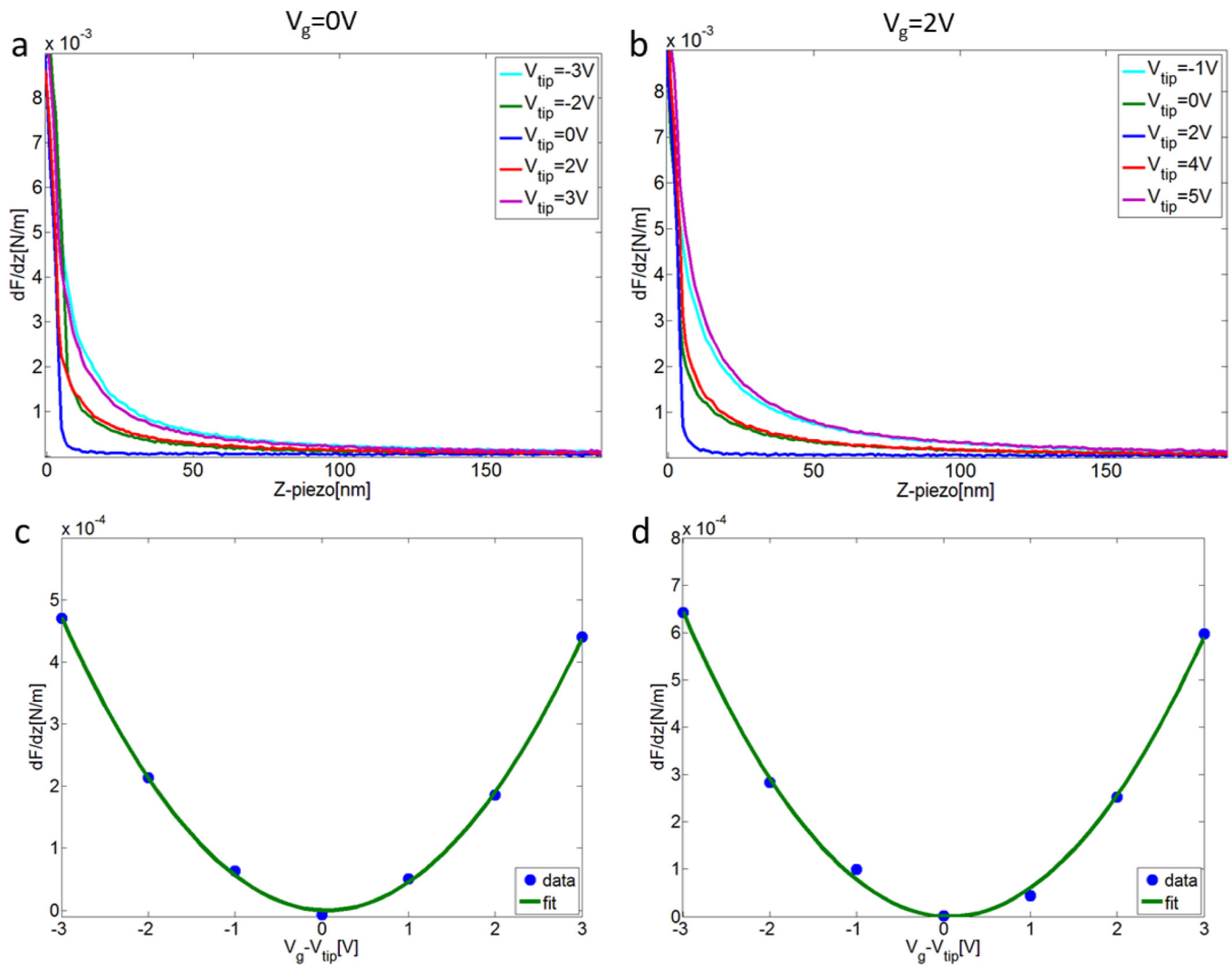


FIG. 3. $\frac{\partial F}{\partial z}$ as a function of z for different V_{tip} values, for $V_g = 0V$ (a) and $V_g = 2V$ (b). $\frac{\partial F}{\partial z}$ at $z = 100$ nm as a function of $V_g - V_{tip}$ for $V_g = 0V$, $V_{tip} = -3, -2, -1, 0, 1, 2, 3V$ (c) and for $V_g = 2V$, $V_{tip} = -1, 0, 1, 2, 3, 4, 5V$ (d). Error bars are smaller than the markers.

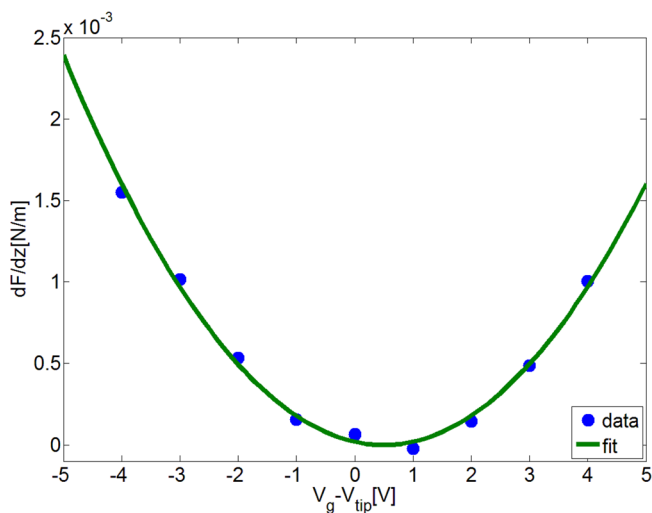


FIG. 4. $\frac{\partial F}{\partial z}$ at $z = 100$ nm as a function of $V_g - V_{tip}$ ($V_g = 0V$, $V_{tip} = -4, -3, -2, -1, 0, 1, 2, 3, 4V$), for a wafer which has undergone 10 min of ozone treatment. Error bars are smaller than the markers.

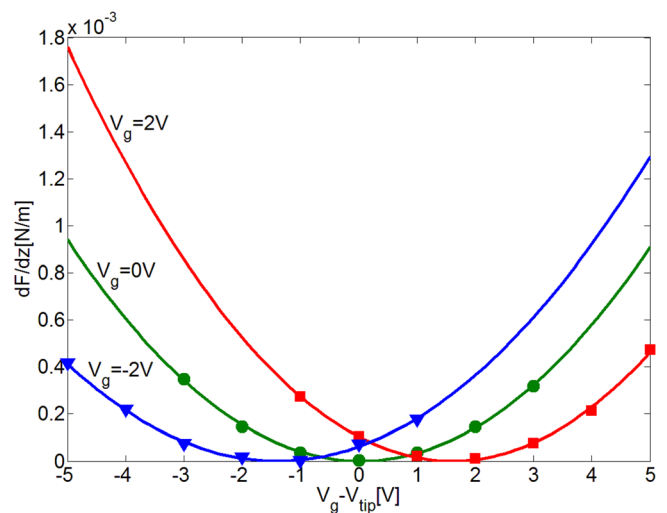


FIG. 5. $\frac{\partial F}{\partial z}$ at $z = 100$ nm as a function of $V_g - V_{tip}$ for $V_g = 2V$ (red squares), $0V$ (green circles), and $-2V$ (blue triangles). $V_{tip} = -3, -2, -1, 0, 1, 2, 3V$. Error bars are smaller than the markers.

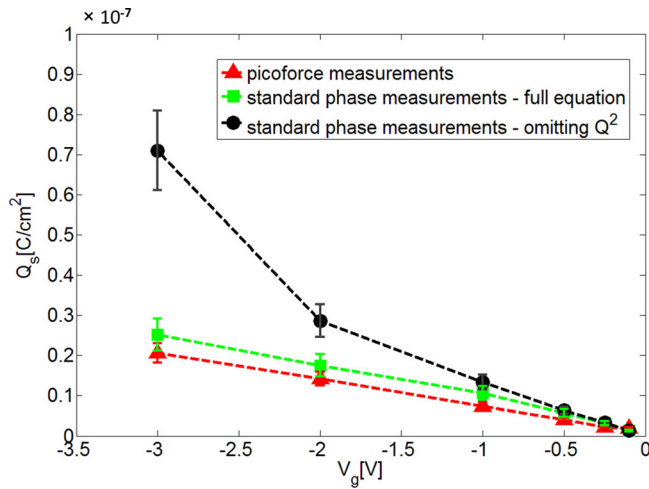


FIG. 6. Q_s calculated in 3 different ways: (1) extracted from the parabolas obtained for each V_g using the force curve-based method (red triangles), (2) calculated from Eq. (6) after measuring the phases using a standard EFM measurement for each V_g (green squares), (3) same as 2, but this time omitting Q_s^2 term from Eq. (6) (black circles).

The induced surface charge distribution which depends on gate voltages immediately hints towards temporal dependence as well, and a possible cause for the hysteresis phenomenon in nano-scale systems. In order to unveil the mechanism through which V_g induces surface charges on the SiO_2 surface, additional experiments were conducted.

First, we performed measurements of the charge distribution in between two grounded electrodes as a function of time, upon changing V_g from 0 V to -2 V at $t=0$ s. Charge measurements were performed using the force-curve based method, as was described previously. As shown in Fig. 7(a), charge accumulates at the examined point according to $Q_s \propto 1 - e^{-t/\tau}$ ($R^2 > 0.998$), indicating an electrical drift-based process. At 500 s, the amount of accumulated charge is approximately $1.5 \times 10^{-8} \pm 1.5 \times 10^{-9} \text{ C/cm}^2$. We repeated the measurement under different ambient humidity conditions (Fig. 7(a)) and found that while the exponential dependence was maintained in all of the measurements, τ reduced drastically when the humidity percentage increased. In order to further explore this matter, we covered the SiO_2 surface between the electrodes with a thin layer (< 100 nm) of PMMA that was baked on a hot plate for 24 h in order to remove any residues of water and performed the measurement again. This time, the extracted charge density was ten times smaller than before and remained constant throughout the measurement (Fig. 7(a)). These results suggest that water molecules that adhere to the surface in ambient conditions facilitate the movement of mobile charges on the SiO_2 . This observation is in agreement with previous findings, which have reported that humidity affects hysteresis significantly.^{26–28}

Similar curves to those depicted in Fig. 7 were found when the gate bias was swept back from -2 V to zero. However, instead of charging behavior, Q_s decayed exponentially with time, which again reflects the significance of the lateral electric fields distribution. These electric fields will depend on the distances from the grounded electrodes as well.

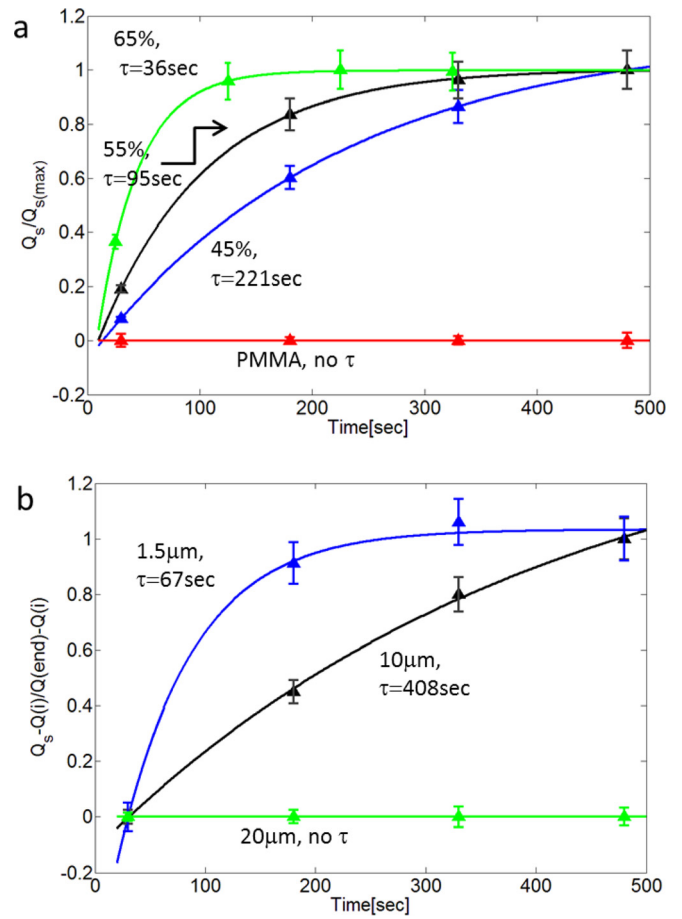


FIG. 7. (a) Measured Q_s between the two electrodes as a function of time upon applying $V_g = -2$ V (at $t=0$ s) for different humidity conditions. $Q_{s(max)} = 1.5 \cdot 10^{-8} \frac{\text{C}}{\text{cm}^2}$. Continuous lines are best fits to exponential time dependence, (b) $\frac{Q_s - Q_i}{Q_{s(end)} - Q_i}$ as a function of time upon applying $V_g = -2$ V (at $t=0$ s) at different distances from grounded electrode, as labeled in the plot. Q_i and Q_{end} are the initial and final measured Q_s . Continuous lines are best fit to exponential time dependence.

Therefore, another experiment was designed to examine the effect of these distances on the charge accumulation process. As before, V_g was changed at $t=0$ s from 0 V to -2 V, and the accumulated charge was measured as a function of time at different distances from a single grounded electrode (Fig. 7(b)). One can observe that τ increases as the distance from the electrode increases as well. At a distance of $20 \mu\text{m}$ from the electrode, charge does not accumulate at all, as was the case in the absence of grounded electrodes (see Fig. 3).

Although the probability of field emission of charge from the electrodes to the surface is extremely small because of the relatively low external applied voltages, we performed an experiment to examine this possibility. Previously we reported that covering the whole sample with a thin layer of PMMA and baking it for 24 h reduced completely any temporal changes in the charge accumulation. This time, the electrode itself and the area adjacent to it were passivated with a thick layer of photoresist, baked for 24 h, and the same measurement was repeated. As expected, the same exponential temporal dependence of the surface charge was observed, indicating that field emission is not the mechanism responsible for the gate induced charge accumulation phenomenon.

The data presented above suggest that gate-induced surface charge redistribution phenomenon takes place only in the vicinity of grounded electrodes and is assisted by water molecules. Furthermore, it has been shown that this charge accumulation process is an electrical drift based process. Since the possibility of field emission of charge from the electrodes to the surface was ruled out, we argue that the observed phenomenon results simply from redistribution of charge which already exists on the surface upon applying gate bias.

To elucidate the above mentioned observations, we propose the following model: Applying non zero gate bias results with lateral electric field lines in the vicinity of metallic electrodes. Under these lateral electric fields, opposite signed mobile charge drifts across the SiO₂ surface and gradually screens the gate. This movement of the charges is facilitated by the water layer which exists on the sample surface at ambient conditions and results in a lower energetic configuration of the electric field lines in the system. A schematic of this gate-induced charge distribution process is given in Fig. 8.

A simplified model for the temporal charging and discharging phenomena can be described as follows: a thin slab on top of the sample surface between the two electrodes behaves as two leaky capacitors. For each capacitor one plate is near one of the electrode, and the other plate is in the middle between the two electrodes. If $\rho(t)$ is the charge density

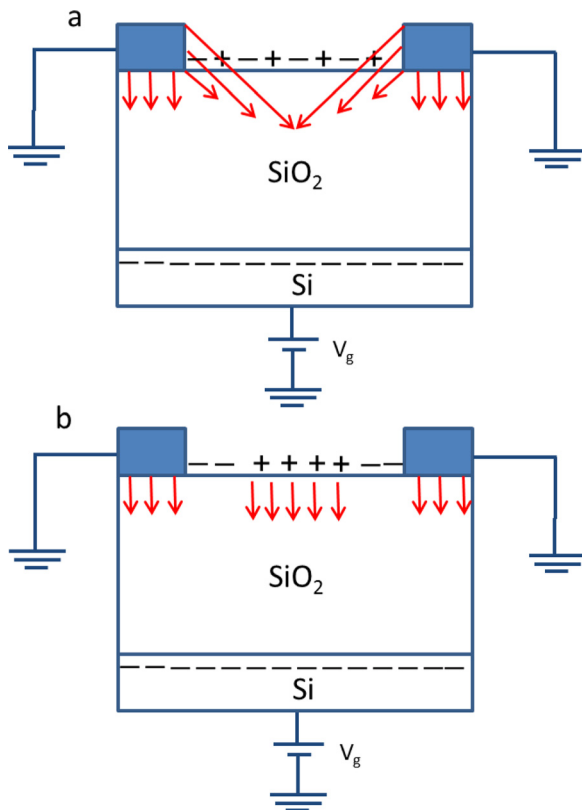


FIG. 8. Schematic presentation of the suggested model. (a) Upon applying V_g to the gate, electric field lines are created in the system due to the charged electrodes. Under the influence of their lateral components, surface charges start drifting and redistributing across the SiO₂. This movement is assisted by water layers on the surface. (b) Final surface charge distribution.

per unit area on one of the plates, then using continuity, Ohm, and Gauss equations one can write the following expression:

$$\frac{d\rho(t)}{dt} = -J = -\sigma E_x = -\sigma \frac{\rho}{\epsilon_0 \epsilon_{ox}}, \quad (8)$$

where J , σ , and E_x are the current density, conductivity, and lateral component of the electric field in the slab, respectively. The solution for this equation has an exponential behavior which is consistent with the experimental results exhibited so far, with time constant, $\tau = \epsilon_0 \epsilon_{ox} / \sigma$.

However, in this derivation, a simplified assumption was done in the relation between E_x and ρ . Thus, in order to examine the validity of the model more accurately, we used a finite element analysis software (COMSOL Multiphysics 4.2a) to perform physical simulations of our system. The obtained results confirm our model very well: Fig. 9(a) shows a snapshot of the electrical potential and electrical field lines in the vicinity of one of the electrodes after a period of time which corresponds to half way through the charge accumulation process. One can see that the charge on the SiO₂ surface move in the expected direction, with exponential time dependence, which eventually results in screening of the gate potential. Fitting the simulated data to the experimental one (performed between the two electrodes with 65% humidity) yields the conductivity of the

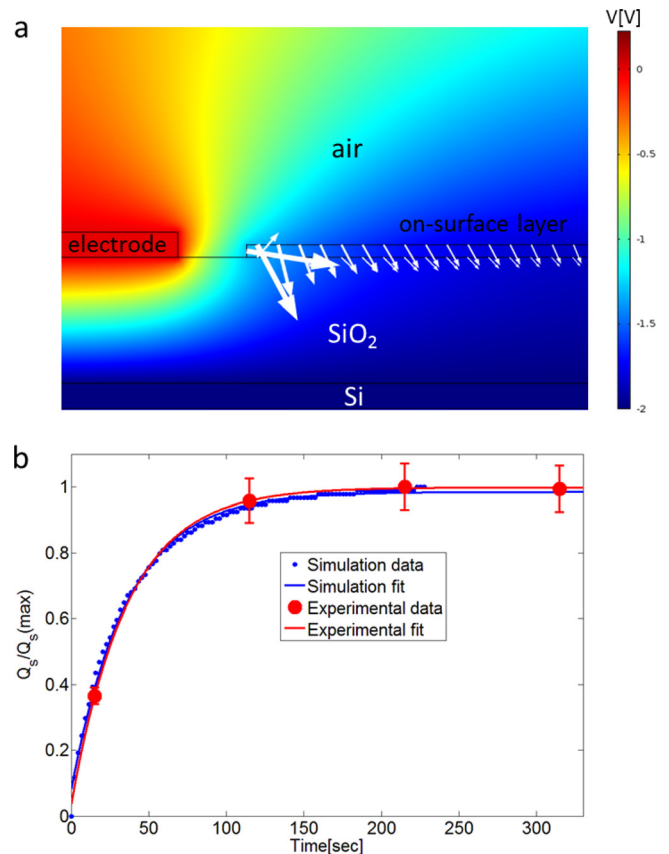


FIG. 9. Simulation results. (a) A snapshot of the electrical potential (color plot) and electrical field lines (white lines) in the vicinity of one of the electrodes half way through the charge accumulation process while applying $V_g = -2$ V to the gate electrode. (b) Experimental charge accumulation vs time (red) and simulation results (blue).

SiO₂, $\sigma = 4.1 \times 10^{-12} \pm 3.5 \times 10^{-13}$ (S/m), with σ as a single fitting parameter for the exponential time dependence (see Fig. 9(b)). The reported range of SiO₂ conductivity is $\sigma = 10^{-12} - 10^{-16}$ (S/m), which is in good agreement with our result. We suggest that the relatively improved conductivity in our system is caused by the water layer which exists on the surface of SiO₂ in ambient conditions.

IV. CONCLUSIONS

In the present study we have developed a force curve EFM based method to gain quantitative information on the temporal and lateral distribution of surface charges on insulating layers. In previous reports, it has been necessary to determine the tip-surface capacitance and its derivatives in order to perform quantitative analysis of the surface charge distribution. This has been a problematic task (as the tip-surface configuration is geometrically complex) that resulted in inevitable approximations which have rendered the quantification of the charge less accurate. The use of the suggested method makes the need to determine the tip-surface capacitance and its derivatives unnecessary. Furthermore, it also enables the accurate determination of the vertical distance between the tip and the surface, a parameter which is critical for the correct quantification of the charge as well.

Using this method, we have been able to quantify spatial and temporal SiO₂ surface charge distribution under different humidity conditions and proved that the gate voltage compliance induces surface charge redistribution which takes place in the vicinity of grounded electrodes and is assisted by water molecules. This redistribution process, during which opposite-signed mobile charge drifts across the SiO₂ surface and gradually screens the applied external gate voltage, is derived by the lateral components of the electric field in the vicinity of the electrodes and results in a lower energetic configuration of the electric field lines in the system. The temporal behavior for this phenomenon follows exponential time dependence with a single time constant which is inversely proportional to the surface conductivity and humidity. A finite element analysis, performed with COMSOL Multiphysics software, supports our conclusions. We believe that the hysteresis phenomenon which is often observed in nano-scale devices and systems at low sweeping gate voltages and has remained an unresolved issue so far is largely caused by this phenomenon.

Moreover, various sensing mechanisms that were suggested for nano-scale devices on top of insulating substrates should be reconsidered regarding our results. We argue that different analytes that modify the transfer characteristic of nano-devices, such as carbon nanotubes or silicon nanowires, may alter the insulating substrates conductivity and, as a result, affect the device conductance. This possibility paves the way to much more sensitive detectors that are sensitive to the substrates conductivity and not only to their own sensing area.

ACKNOWLEDGMENTS

The authors thank Professor Y. Eichen for fruitful discussions. The work was supported by the Russell Berrie

Nanotechnology Institute, the Micro-Nano Fabrication Unit at the Technion, and the ISF (Grant No. 1334/06).

- ¹M. Nonnenmacher, M. P. O'Boyle, and H. K. Wickramasinghe, "Kelvin probe force microscopy," *Appl. Phys. Lett.* **58**, 2921–2923 (1991).
- ²J. Lambert, C. Guthmann, and M. Saint-Jean, "Relationship between charge distribution and its image by electrostatic force microscopy," *J. Appl. Phys.* **93**, 5369–5376 (2003).
- ³K. Domansky, Y. Leng, C. C. Williams, J. Janata, and D. Petelenz, "Mapping of mobile charges on insulator surfaces with the electrostatic force microscope," *Appl. Phys. Lett.* **63**, 1513–1515 (1993).
- ⁴M. Paillet, P. Poncharal, and A. Zahab, "Electrostatics of Individual single-walled carbon nanotubes investigated by electrostatic force microscopy," *Phys. Rev. Lett.* **94**, 186801 (2005).
- ⁵C. Staii, A. T. Johnson, and N. J. Pinto, "Quantitative analysis of scanning conductance microscopy," *Nano Lett.* **4**, 859–862 (2004).
- ⁶A. Bachold, M. S. Fuhrer, S. Plyasunov, M. Forero, E. H. Anderson, A. Zettl, and P. L. McEuen, "Scanned probe microscopy of electronic transport in carbon nanotubes," *Phys. Rev. Lett.* **84**, 6082–6085 (2000).
- ⁷M. Bockrath, N. Markovic, A. Shepard, M. Tinkham, L. Gurevich, L. P. Kouwenhoven, M. W. Wu, and L. L. Sohn, "Scanned conductance microscopy of carbon nanotubes and lambda-DNA," *Nano Lett.* **2**, 187–190 (2002).
- ⁸J. Kim, W. Jasper, R. Barker, and J. Hinestroza, "Application of electrostatic force microscopy on characterizing an electrically charged fiber," *Fibers Polym.* **11**, 775–781 (2010).
- ⁹T. Melin, D. Deresmes, and D. Stievenard, "Charge injection in individual silicon nanoparticles deposited on a conductive substrate," *Appl. Phys. Lett.* **81**, 5054–5056 (2002).
- ¹⁰C. Y. Ng, T. P. Chen, H. W. Lau, Y. Liu, M. S. Tse, O. K. Tan, and V. S. W. Lim, "Visualizing charge transport in silicon nanocrystals embedded in SiO₂ films with electrostatic force microscopy," *Appl. Phys. Lett.* **85**, 2941–2943 (2004).
- ¹¹D. M. Schaadt, E. T. Yu, S. Sankar, and A. E. Berkowitz, "Charge storage in Co nanoclusters embedded in SiO₂ by scanning force microscopy," *Appl. Phys. Lett.* **74**, 472–474 (1999).
- ¹²H. Diesinger, T. Melin, S. Barbet, D. Deresmes, and D. Stievenard, "Electric force microscopy of individually charged semiconductor nanoparticles," *Phys. Status Solidi A* **203**, 1344–1347 (2006).
- ¹³G. H. Buh, H. J. Chung, and Y. Kuk, "Real-time evolution of trapped charge in a SiO₂ layer: An electrostatic force microscopy study," *Appl. Phys. Lett.* **79**, 2010–2012 (2001).
- ¹⁴J. Lambert, G. de Loubens, C. Guthmann, M. Saint-Jean, and T. Melin, "Dispersive charge transport along the surface of an insulating layer observed by electrostatic force microscopy," *Phys. Rev. B* **71**, 155418 (2005).
- ¹⁵J. Lambert, C. Guthmann, C. Ortega, and M. Saint-Jean, "Permanent polarization and charge injection in thin anodic alumina layers studied by electrostatic force microscopy," *J. Appl. Phys.* **91**, 9161–9169 (2002).
- ¹⁶C. Guillemot, P. Budau, J. Chevrier, F. Marchi, F. Comin, C. Alandi, F. Bertin, N. Buffet, C. Wyon, and P. Mur, "Imaging of stored charges in Si quantum dots by tapping and electrostatic force microscopy," *Europhys. Lett.* **59**, 566–571 (2002).
- ¹⁷M. J. Gordon and T. Baron, "Amplitude-mode electrostatic force microscopy in UHV: Quantification of nanocrystal charge storage," *Phys. Rev. B* **72**, 165420 (2005).
- ¹⁸M. Zdrojek, T. Melin, H. Diesinger, D. Stievenard, W. Gebicki, and L. Adamowicz, "Charging and discharging processes of carbon nanotubes probed by electrostatic force microscopy," *J. Appl. Phys.* **100**, 114326 (2006).
- ¹⁹M. Zdrojek, T. Melin, C. Boyaval, D. Stievenard, B. Jouault, M. Wozniak, A. Huczko, W. Gebicki, and L. Adamowicz, "Charging and emission effects of multiwalled carbon nanotubes probed by electric force microscopy," *Appl. Phys. Lett.* **86**, 213114 (2005).
- ²⁰T. S. Jespersen and J. Nygard, "Charge trapping in carbon nanotube loops demonstrated by electrostatic force microscopy," *Nano Lett.* **5**, 1838–1841 (2005).
- ²¹S. Hudlet, M. Saint Jean, C. Guthmann, and J. Berger, "Evaluation of the capacitive force between an atomic force microscopy tip and a metallic surface," *Eur. Phys. J. B* **2**, 5–10 (1998).
- ²²F. Marchi, R. Dianoux, H. Smilde, P. Mur, F. Comin, and J. Chevrier, "Characterisation of trapped electric charge carriers behaviour at nanometer scale by electrostatic force microscopy," *J. Electrostat.* **66**, 538–547 (2008).

- ²³G. Qi, Y. Yang, H. Yan, L. Guan, Y. Li, X. Qiu, and C. Wang, "Quantifying surface charge density by using an electric force microscope with a referential structure," *J. Phys. Chem. C* **113**, 204–207 (2009).
- ²⁴J. Kim, W. J. Jasper, and J. P. Hinestroza, "Charge characterization of an electrically charged fiber via electrostatic force microscopy," *J. Eng. Fiber Fabr.* **1**, 30–46 (2006).
- ²⁵G. C. Qi, H. Yan, L. Guan, Y. L. Yang, X. H. Qiu, C. Wang, Y. B. Li, and Y. P. Jiang, "Characteristic capacitance in an electric force microscope determined by using sample surface bias effect," *J. Appl. Phys.* **103**, 114311 (2008).
- ²⁶W. Kim, A. Javey, O. Vermesh, Q. Wang, Y. Li, and H. Dai, "Hysteresis caused by water molecules in carbon nanotube field-effect transistors," *Nano Lett.* **3**, 193–198 (2003).
- ²⁷P. S. Na, H. Kim, H.-M. So, K.-J. Kong, H. Chang, B. H. Ryu, Y. Choi, J.-O. Lee, B.-K. Kim, J.-J. Kim *et al.*, "Investigation of the humidity effect on the electrical properties of single-walled carbon nanotube transistors," *Appl. Phys. Lett.* **87**, 093101 (2005).
- ²⁸M. Rinkio, M. Y. Zavodchikova, P. Torma, and A. Johansson, "Effect of humidity on the hysteresis of single walled carbon nanotube field-effect transistors," *Phys. Status Solidi B* **245**, 2315–2318 (2008).